Earth and Planetary Science Letters 562 (2021) 116839

Contents lists available at ScienceDirect

Earth and Planetary Science Letters

www.elsevier.com/locate/epsl

Periodic oceanic euxinia and terrestrial fluxes linked to astronomical forcing during the Late Devonian Frasnian–Famennian mass extinction

Man Lu [a], YueHan Lu [a,*], Takehitio Ikejiri [a], Dayang Sun [b], Richard Carroll [c], Elliot H. Blair [d], Thomas J. Algeo [e,f], Yongge Sun [b,*]

[a] Molecular Eco-Geochemistry Laboratory, Department of Geological Sciences, University of Alabama, Tuscaloosa, AL 35485, USA
[b] Organic Geochemistry Unit, School of Earth Science, Zhejiang University, Hangzhou, Zhejiang 310027, China
[c] Energy Investigation Program, Geological Survey of Alabama, Tuscaloosa, AL 35401, USA
[d] Department of Anthropology, University of Alabama, Tuscaloosa, AL 35487, USA
[e] Department of Geology, University of Cincinnati, Cincinnati, OH 45221-0013, USA
[f] State Key Laboratories of GPMR and BGEG, China University of Geosciences, Wuhan, Hubei 430074, China

ARTICLE INFO

Article history:
Received 17 September 2020
Received in revised form 16 January 2021
Accepted 16 February 2021
Available online xxxx
Editor: L. Derry

Keywords:
Chattanooga Shale
Upper Kellwasser
black shale
biomarker
eccentricity
precession

ABSTRACT

Oceanic anoxia is considered as the immediate cause of the Frasnian–Famennian mass extinction, yet the frequency of anoxia and associated environmental modulators remains unknown. Here, we demonstrate that astronomical forcing paced oceanic anoxic episodes by mediating land-ocean interactions during the Upper Kellwasser (UKW) Event, using an ultra-high-resolution (one centimeter spacing), multi-proxy geochemical profile of a UKW interval from the Upper Devonian Chattanooga Shale of Tennessee, USA. Organic and inorganic geochemical indices for oceanic anoxia/euxinia, marine primary productivity, terrestrial plant/soil inputs, and clastic sediment inputs show synchronous fluctuations that were paced by the Earth's orbital precession. This study provides the first mechanistic evidence linking the periodicity of Late Devonian oceanic euxinia to astronomical forcing and identifies terrestrial-to-marine inorganic and organic fluxes as the driver of this linkage. These results suggest that astronomical forcing modulated the expression of environmental stressors that led to the Frasnian–Famennian mass extinction.

1. Introduction

Of the Big Five mass extinctions of the Phanerozoic, the Late Devonian Frasnian–Famennian (F–F) biotic crisis is known for its severe impacts on tropical shallow marine faunas (Bambach et al., 2004). The ultimate cause proposed for this biocrisis remains in debate, including bolide impacts (Sandberg et al., 2002), sea-level fluctuations (Copper, 2002), climate change (Joachimski et al., 2002), volcanism (Racki et al., 2018), tectonism (Averbuch et al., 2005) and land plant evolution (Algeo and Scheckler, 1998). However, a wide consensus exists that ocean anoxia, caused by eutrophication and/or stratification, was the immediate, direct cause, based on widespread deposition of organic-rich sediments contemporaneous with marine biodiversity losses across the F–F boundary (e.g., Joachimski and Buggisch, 1993). Worldwide deoxygenation is proposed to have occurred in the late Frasnian seas, and recent geochemical and sedimentological results demonstrate that anoxic/euxinic events occurred episodically in shallow epeiric seas during the Late Devonian (Fig. 1; Supplementary Table S1). The episodic nature of anoxia matches well with paleontological evidence that biodiversity losses during the F–F biotic crisis were due to recurring environmental stresses to which marine life was unable to adapt, resulting in extraordinarily low rates of species origination (Bambach et al., 2004; Boyer et al., 2014). However, the frequency and duration of oceanic anoxic events, as well as the mechanisms that initiated and regulated these episodes, have not been determined to date (Carmichael et al., 2019).

Here we test the hypothesis that astronomical forcing controlled the frequency of oceanic anoxic episodes by altering land surface processes and terrestrial-marine biogeochemical linkage during the Late Devonian Upper Kellwasser (UKW) event. The F–F biotic crisis was characterized by a series of extinction pulses, among which the largest in shallow-marine ecosystems occurred during the UKW event (House, 2002). Although astronomical forcing has been identified as a key driver regulating variation in lithofacies and geochemical proxies throughout the Devonian (e.g., De Vleeschouwer et al., 2013, 2017; Elrick et al., 2009; Liu et al., 2019), the role of astronomical forcing during mass extinction events remains poorly understood. De Vleeschouwer et al. (2017) were the first who identified a strong obliquity signal in six glob-

* Corresponding authors.
E-mail addresses: yuehan.lu@ua.edu (Y. Lu), ygsun@zju.edu.cn (Y. Sun).

https://doi.org/10.1016/j.epsl.2021.116839
0012-821X/

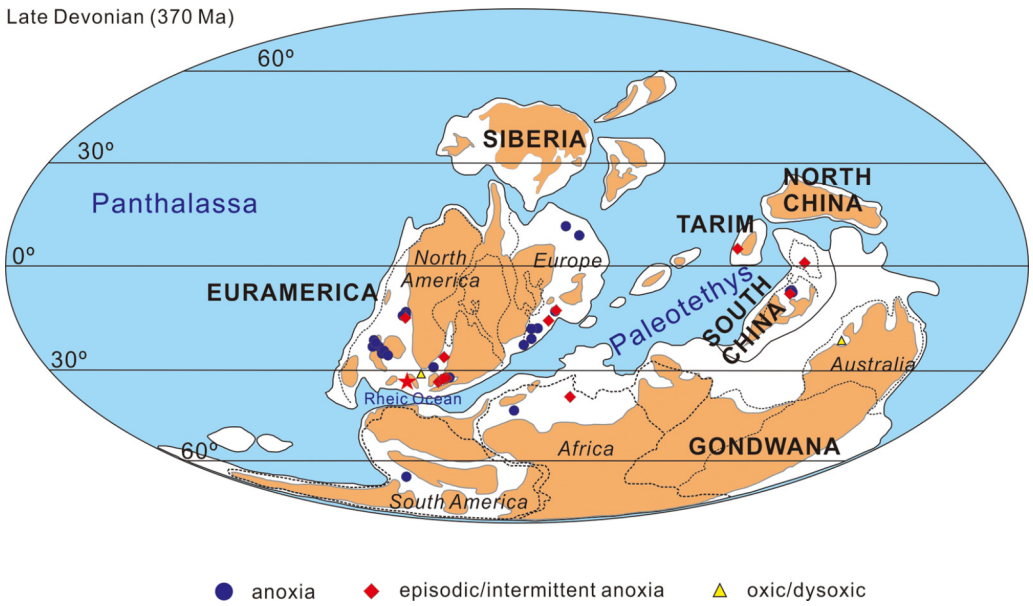

Fig. 1. Late Devonian global paleogeography showing the location of the Upper Kellwasser (UKW) sections with reported redox data. Late Devonian global paleogeographic map (370 Ma) is adapted from Golonka (2020). Red star denotes the present study site, the Chestnut Mound outcrop of the Chattanooga Shale; circles denote the locations of UKW intervals reported from previous studies. To date, 92 studies of 46 UKW sections have been published, with 18 sections showing intermittent anoxia, 2 sections showing oxic/dysoxic conditions, and 26 sections with anoxia of indeterminate duration (i.e., no clear indication of permanent or episodic). A brief summary of the method and results of our literature compilation is available in Supplementary Materials, and the paleogeographic locations, lithologic descriptions, and depositional environments of the 46 UKW sections are given in Supplementary Table S1. (For interpretation of the colors in the figure(s), the reader is referred to the web version of this article.)

ally distributed stable carbon isotopic values ($\delta^{13}C$) profiles of the UKW interval. This observation prompted the authors to speculate that the timing of the outbreak of the extinction intervals may be controlled by astronomical configurations, although the ultimate cause is linked to processes that alter the global carbon cycle. Biogeochemical mechanisms that could drive the link between astronomical forcing and carbon cycle, however, have not been elucidated. In the present study, we present an ultra-high-resolution (1-cm spacing), multi-proxy geochemical profile from the UKW interval of a Chattanooga Shale outcrop in the southern Appalachian Basin, Tennessee, USA. We probe potential links between astronomical forcing and episodic oceanic anoxia and identify terrestrial and marine biogeochemical drivers mediating the links during the UKW interval. Our results provide the first multi-proxy, mechanistic evidence demonstrating that the frequency and magnitude of marine anoxic events were controlled by the frequency and magnitude of land-sea interactions that were modulated by astronomical forcing across the UKW interval, offering new insights into the causative mechanism(s) of the F–F mass extinction.

2. Geological setting

The Chattanooga Shale was deposited in an epicontinental sea from the early Frasnian to late Famennian (Li and Schieber, 2015). The study section of the Chattanooga Shale is located at Chestnut Mound, central Tennessee (36.207838°N, 85.834365°W; Fig. 1). The 7.25-m-thick outcrop exposes both the Frasnian-age Dowelltown Member and Famennian-age Gassaway Member of the Chattanooga Shale (Fig. 2, a detailed description of stratigraphic and lithological features can be found in Li and Schieber (2015). The presence of UKW interval in this outcrop is evidenced by (i) the latest Frasnian conodonts (i.e., *Palmatolepis linguiformis*) (Over, 2007), (ii) a volcanic ash bed (i.e., the Center Hill Ash; Over, 2002) near the top of the MN 13 Zone, (iii) a pronounced positive excursion (>2‰) of stable carbon isotopic values of organic matter ($\delta^{13}C_{org}$) within the uppermost Frasnian MN 13 Zone, followed by a negative shift through the lower Famennian (Fig. 2), and (iv) an increase in C_{28}/C_{29} sterane ratios within the uppermost Frasnian MN 13 Zone (Fig. 2). Positive excursions in both organic carbon and carbonate have been used as chemostratigraphic markers for the UKW globally (e.g., De Vleeschouwer et al., 2017), although the shapes and amplitudes of these excursions as well as their stratigraphic positions relative to the F–F boundary are variable (Carmichael et al., 2019). The positive $\delta^{13}C_{org}$ excursion observed in the uppermost MN 13 Zone here correlates well with those records from some UKW sections in Europe (e.g., Joachimski and Buggisch, 1993) and North America (e.g., Sageman et al., 2003; Whalen et al., 2017). A similar spike in C_{28}/C_{29} sterane ratios has also been reported as a marker in other upper Frasnian sections (Schwark and Empt, 2006; Haddad et al., 2016), further supporting the identification of the UKW in the study section.

3. Materials and methods

3.1. Sample collection

Thirty samples were collected at an interval of ~25 cm throughout the 7.25-m-thick Chattanooga Shale exposure of the Chestnut Mound section and additional thirty-five samples were collected at an interval of 1 cm from the UKW interval. In addition, 193 samples were collected at 2–3 cm intervals from the base to 4 m of the Chattanooga Shale. Surface and weathered rocks were removed before sampling. Prior to geochemical analyses, the surface of each sample was further removed in the lab by knife, and only freshly exposed pieces were used for subsequent analyses. All samples were washed using ultra-pure carbon-free water.

3.2. Bulk geochemistry

Prior to the analysis of total organic carbon (TOC) and $\delta^{13}C_{org}$, all samples were ground into a 100–200 mesh powder. Approximately 10 mg of black shale or 20 mg of gray-greenish shale sample was placed into a tin capsule and decarbonated with 5% sulfurous acid. All samples were dried overnight in an oven at

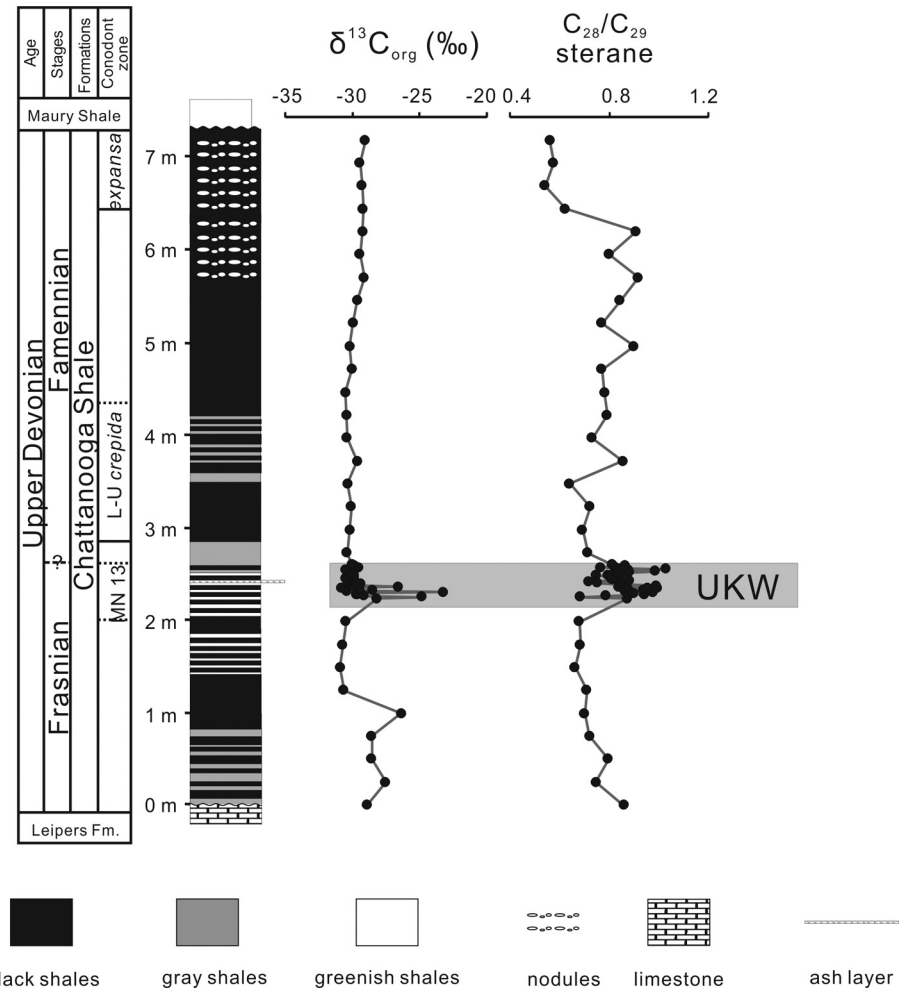

Fig. 2. Stratigraphic column, $\delta^{13}C_{org}$ and C_{28}/C_{29} sterane ratios of the Chestnut Mound outcrop of the Chattanooga Shale, central Tennessee. Lithostratigraphy is modified after Li and Schieber (2015), and the conodont biostratigraphy is from Over (2007). Gray bar highlights the Upper Kellwasser (UKW) interval.

50 °C. The samples were then submitted to the University of California Davis Stable Isotope Facility (California, USA) and analyzed on a Micro Cube elemental analyzer (Elementar Analysensysteme GmbH, Hanau, Germany) interfaced to a PDZ Europa 20–20 isotope ratio mass spectrometer (The Sercon Ltd., Cheshire, UK). $\delta^{13}C_{org}$ values (‰) were calibrated against NIST Standard Reference Materials (USGS-40, USGS-41) and reported relative to V-PDB. The analytical precision was less than 0.2‰ based on internal standards that included nylon, bovine liver, peach leaves, and glutamic acid.

Trace element concentrations of 35 samples were measured at the ALS Chemex Lab, Ltd (Guangzhou, China). Two to five milligrams of grounded sample was treated using a three-acid (HF-HNO_3-$HClO_4$) digestion method. The residue was then leached with HCl. The analysis of the solution was conducted using a PerkinElmer Elan9000 element inductively coupled plasma mass spectrometer (ICP-MS). The analytical precision for all trace elements was better than 7%.

We also measured bulk elemental compositions of all collected samples using the Bruker Tracer III-SD hand-held XRF under vacuum. These data were used only for the time series analysis described below. Three measurements were taken on a fresh surface of each sample with source energy of 15 keV (no filter, 25 μA) and 180-seconds count time. Element intensities were obtained by measuring the peak area of raw X-ray spectra using the ARTAX software. The ratio between titanium and aluminum counts (Ti/Al) was calculated.

3.3. Biomarker analysis

Sixty-five samples were processed for molecular biomarker analyses. About 20 grams of powdered sample material were Soxhlet-extracted with a mixture of Dichloromethane (DCM)/Methanol (MeOH) (97:3, v/v) for at least 72 h. Activated copper was added to remove the elemental sulfur. The extracts were concentrated using a rotary evaporator and transferred into a preweighed 4 mL vial. Each sample was subsequently separated into aliphatic, aromatic, and polar fractions by silica gel column chromatography with a mixture of activated silica gel and alumina (3:1, v/v). The aliphatic fraction was eluted with petroleum ether (4 column volumes) followed by the aromatic fraction eluted with benzene and the polar fraction eluted with MeOH. Each of these fractions was collected and dried via rotary evaporation and then diluted with 1 mL of hexane. The saturated fraction of each sample was then separated into straight alkane and branched/cyclic alkane (b/c) fractions through urea adduction.

The aliphatic fraction was quantified on an Agilent 7890A gas chromatograph (GC) equipped with a flame ionization detector (FID) and a DB-1MS capillary column (60 m×0.32 mm, 0.25 μm film thickness). The initial oven temperature was 60 °C, maintained for 2 min, and increased at 4 °C/min to 295 °C, maintained for 30 min. Nitrogen was the carrier gas at a flow rate of 1.0 ml/min. The inlet temperature was set at 295 °C and FID temperature was 300 °C. Normal alkanes were quantified by their peak areas relative to an internal standard (n-$C_{24}D_{50}$) added prior to GC-FID

measurement. The branched/cyclic alkane and aromatic fractions were analyzed on an Agilent 7890B GC-5977A mass spectrometer (MS) equipped with a DB-1MS capillary column (60 m×0.32 mm, 0.25 μm film thickness). Using helium as the carrier gas (1.0 ml/min), GC-oven was heated from 80 °C with a 2 min hold to 220 °C at 3 °C /min and further increased to 300 °C at 2 °C /min with a 30 min hold. The source was operated in 70 eV electron impact mode at 230 °C. Compounds were identified by mass spectra and relative retention times. Selected ion monitoring (SIM) was used for quantifying steranes (m/z = 217) in branched/cyclic alkane fraction and aryl isoprenoids (m/z = 133) in aromatic fraction. For the quantification of aromatic fractions, known amounts of phenanthrene-D10 and dibenzothiophene-D8 were added prior to GC-MS measurement.

3.4. Time-series analysis

The detection and interpretation of major Milankovitch cycles were conducted on the 193 samples collected at 2–3 cm intervals from the Upper Frasnian to Lower Famennian interval (4 m thickness). Prior to the analyses, the Ti/Al data were interpolated linearly to a constant 2-cm resolution and subsequently detrended by subtracting a linear trend using the "detrending" toolbox in Acycle v2.1 software (Li et al., 2019).

The time-series analysis of processed Ti/Al data was performed in Acycle v2.1 (Li et al., 2019). Multi-taper method (MTM) (Thomson, 1982) was used with three 2π tapers and a time-bandwidth product of 2. The MTM power spectra of detrended Ti/Al data were tested against first-order autogressive "AR(1)" red-noise models (Mann and Lees, 1996) at 90%, 95%, and 99% confidence levels with a 20% median filter length and linear fitting. Correlation coefficient (COCO) analysis was carried out to evaluate the most likely sedimentation rate for the study section, through comparison between power spectra of proxy series and specific astronomical forcing targets (Li et al., 2019). The most optimal sedimentation rate would correspond to the highest Pearson's correlation coefficient, the lowest significance level of the null hypothesis (H_0), and the largest total number of astronomical parameters (Li et al., 2019). The targeted theoretical astronomical frequencies included main obliquity and precession frequencies (1/34.4 kyr, 1/21.3 kyr, 1/20.2 kyr and 1/17.4 kyr) at 370 Ma (Waltham, 2015) and three orbital eccentricity frequencies (1/405 kyr, 1/128 kyr and 1/95 kyr) (Laskar et al., 2004). The sedimentation rates tested by COCO spanned from 0.05 cm/kyr to 2 cm/kyr with a step of 0.2 cm/kyr. This range of sedimentation rate enclosed the long-term average sedimentation rate determined based on conodonts. According to the Devonian time scale (Kaufmann, 2006), the upper MN 13 biozone (MN 13 b and c) has a duration of ~500 kyr and the MN 13 Zone of the study section spans ~0.8 m (Over, 2007), giving a range of long-term mean sedimentation rate of ~0.2 cm/kyr. The significance of the sedimentation rate was tested using Monte Carlo simulation with 5000 iterations. Based on the sedimentation rates constrained by the COCO analysis, major cycles recognized in the power spectrum were converted from the stratigraphic to time domain and isolated by Gaussian band pass filtering (Kodama and Hinnov, 2014). The filtered 405-kyr and ~21-kyr precession cycles were extracted by Gaussian filtering with passbands of 0.7±0.1 cycles/m and 11.78±0.08 cycles/m, respectively.

The interpreted 405-kyr eccentricity related sedimentary cycles were used to convert data from the stratigraphic to time domain. Prior to subsequent analyses, the 405-kyr tuned data series was linearly interpolated to a uniform sampling interval of 5.8 kyr. To track the presence of eccentricity and precession cycles in the time domain, the 2π MTM analysis was performed on the 405 kyr-tuned data with "AR(1)" model at 90%, 95%, and 99% confidence levels with a 20% median filter length and linear fitting. The Evolutionary Fast Fourier Transform (eFFT) analysis (Kodama and Hinnov, 2014) was performed on the Ti/Al data at the stratigraphic domain to depict spectral features and corresponding cyclicity related to variable sediment accumulation rates. The width of the sliding window was 0.804 m, and each step was set as 0.02 m.

4. Results

4.1. Organic matter characteristics of the UKW interval

Total organic carbon (TOC) contents range from 0.2 to 5.0%, and $\delta^{13}C_{org}$ values were from −30.8 to −23.2‰. Both proxies show high variability through the UKW interval (Fig. 3, A and B). Molecular biomarkers were identified and quantified to reconstruct changes in biological sources or environmental conditions during the deposition of the Chattanooga Shale. Absolute concentrations of biomarkers show greater coefficients of variation than TOC (Supplementary Table S2), demonstrating that variations in TOC-normalized biomarkers are not primarily driven by TOC.

Depositional redox conditions were evaluated using intermediate-chain aryl isoprenoids (C_{18-20}), which were detected in the aromatic fractions of all samples (Supplementary Fig. S1). These compounds can be attributed to carotenoids specific to photosynthetic green sulfur bacteria whose presence is an indicator of photic zone euxinia (PZE) (Grice et al., 2005). Their concentrations vary from 5.2 to 150.6 μg/g TOC and show frequent fluctuations through the upper Frasnian (Fig. 3C).

Marine primary productivity was evaluated using short-chain normal alkanes and C_{27} steranes. The samples yielded normal alkanes with carbon numbers ranging from C_{11} to C_{36} with a peak at *n*-C_{17} or *n*-C_{19} and no odd-over-even predominance from *n*-C_{23} to *n*-C_{31} (Supplementary Fig. S2A). C_{17} and C_{19} *n*-alkanes in low-thermal-maturity rocks indicate primary productivity by algae, phytoplankton, and photosynthetic bacteria (Han et al., 1968). C_{27} steranes are a productivity biomarker that is more specific to red algae (Kodner et al., 2008) (Supplementary Fig. S2B). In the UKW section of the present study, the concentrations of both *n*-C_{17+19} alkanes and C_{27} steranes show frequent fluctuations (Fig. 3, E and F), ranging from 89.6 to 3.8×10^3 μg/g TOC and 1.9 to 54.2 μg/g TOC, respectively. These proxies exhibit significant covariation (Pearson's $r = +0.66$, $P < 0.001$; Supplementary Table S3A), supporting the inference that both indices reflect marine primary productivity.

A suite of organic compounds was used to evaluate contributions from terrestrial plants. Long-chain *n*-alkanes (i.e., C_{27}, C_{29}, and C_{31}) in low-thermal-maturity rocks are commonly employed as a proxy for inputs from vascular plants, with the caveat that some mosses and non-marine algae are also potential sources (Eglinton and Hamilton, 1967; Bush and McInerney, 2013). $C_{27+29+31}$ *n*-alkanes vary from 89.6 to 3.8×10^3 μg/g TOC in the samples (Fig. 3G). Norabietane, retene, and tetrahydroretene are generally interpreted as compounds from abietic acid produced by conifers (Lu et al., 2013), and the presence of abietane-type compounds in Devonian rocks is considered as an indicator of early tracheophytes (Lu et al., 2019). Norabietane was identified in all samples, ranging between 1.9 and 47.3 μg/g TOC (Supplementary Figs. S2C and S3A). Retene and tetrahydroretene were detected in the aromatic fraction (Supplementary Fig. S4), varying in the range of 0.2–4.8 μg/g TOC and 0.7–8.8 μg/g TOC, respectively (Fig. 3H; Supplementary Fig. S3B). These biomarkers are significantly correlated with each other (Pearson's $r \geq +0.38$, $P \leq 0.03$; Supplementary Table S3B), which is consistent with the interpretation that they share terrestrial plants as a common source. In addition, dibenzofuran (DBF) serves as an indirect proxy for terrestrial/soil inputs to marine sediments and has been used to indicate soil erosion intensity of the source areas (Sephton et al., 2005). DBF is

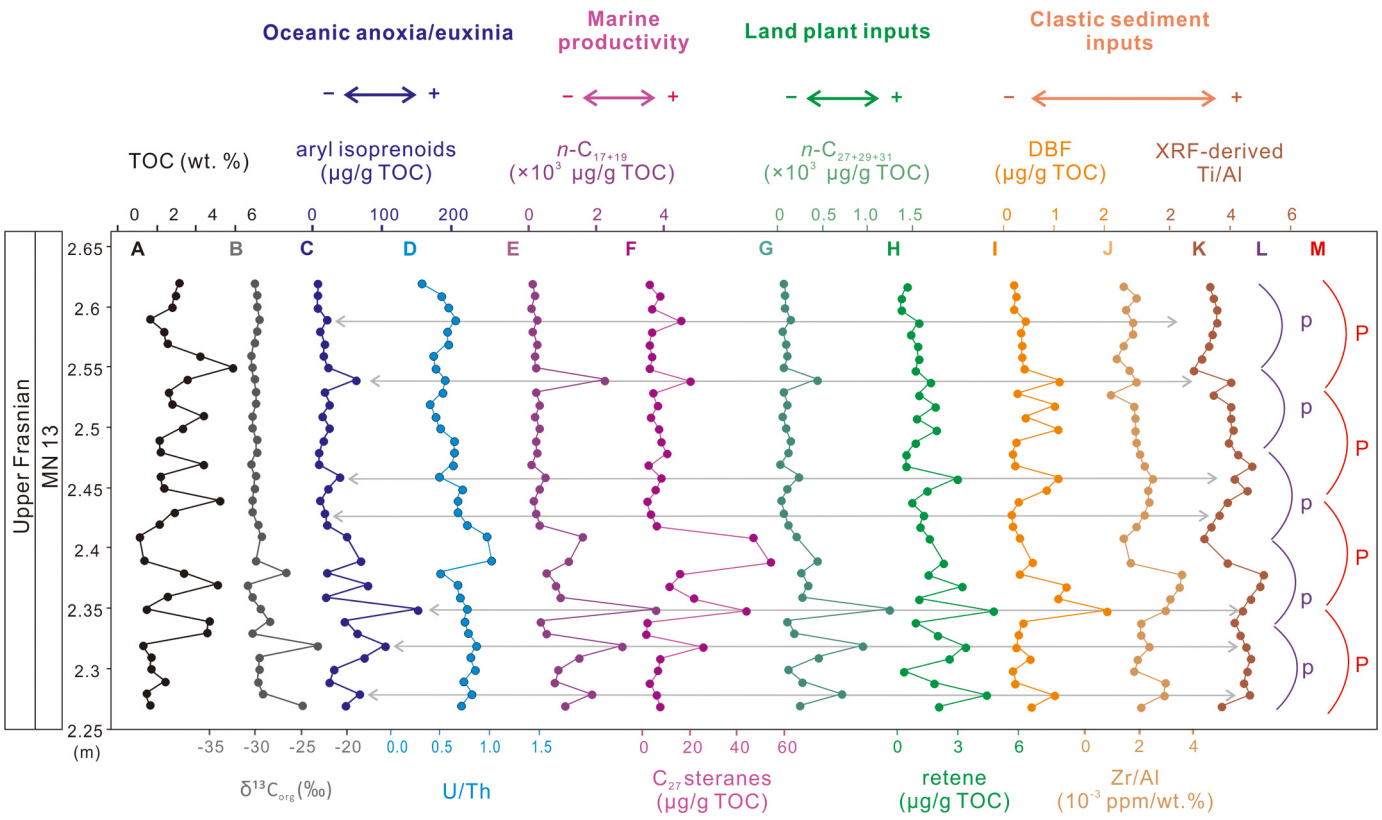

Fig. 3. High-resolution profiles of geochemical proxies measured from the Upper Kellwasser (UKW) interval of the Chestnut Mound outcrop, central Tennessee. (**A**) Total organic carbon (TOC). (**B**) Stable carbon isotopic values of organic matter ($\delta^{13}C_{org}$). (C) C_{18-20} aryl isoprenoids, and (**D**) U/Th are proxies for redox conditions. (**E**) Short-chain normal alkanes (n-C_{17+19} alkanes) and (F) C_{27} steranes are proxies for marine primary productivity. (**G**) long-chain normal alkanes (n-$C_{27+29+31}$ alkanes), (**H**) retene and (**I**) dibenzofuran (DBF) are proxies for terrestrial plant and soil organic matter inputs. (**J**) Zr/Al and (**K**) Ti/Al are proxies for clastic sediment inputs. (**L**) The ~7-cm-thick cycles (purple arcs) are interpreted as the ~17-kyr precession cycle, and (**M**) the ~8–9-cm-thick cycles (red arcs) are interpreted as the 21-kyr precession cycle. The gray lines with double-headed arrows highlight the shifting correlations across various proxies.

thought to derive from multiple terrestrial sources, including dehydrated polysaccharides produced through microbial decay in soils, a lignin source common in woody plants (Fenton et al., 2007), and biomass combustion (Marynowski and Simoneit, 2009). DBF in the study samples fluctuates from 0.1 to 2.0 μg/g TOC (Fig. 3I) and covaries positively with the abovementioned land plant-derived biomarkers (Pearson's $r > +0.46$, $P \leq 0.006$; Supplementary Table S3C).

4.2. Trace elements of the UKW interval

U/Th and V/(V+Ni) ratios are proxies for redox conditions in oceanic bottom waters (e.g., Riquier et al., 2005). U/Th and V/(V+Ni) ratios in the study samples vary from 0.3 to 1.0 and 0.6 to 0.9, respectively (Fig. 3D; Supplementary Fig. S3C). They are both positively correlated with C_{18-20} aryl isoprenoid proxy for PZE through the UKW interval (Pearson's $r > +0.5$, $P \leq 0.001$) (Supplementary Table S3A), confirming that all proxies reflect redox variation. All show fluctuations through the UKW interval, which indicates rapidly changing redox conditions in the ocean (Fig. 3, C and D; Supplementary Fig. S3C).

Ti/Al and Zr/Al ratios can reflect changes in clastic sediment influx, with higher values indicating a larger proportion of silt-fraction heavy minerals that tend to occur under greater riverine discharge (Lash, 2017). In the study section, Zr/Al and Ti/Al ratios vary from 9.6×10^{-4} to 3.6×10^{-3} ppm/wt.% and from 2.8 to 5.1, respectively. Ti/Al covaries positively with Zr/Al (Pearson's $r = +0.78$, $P < 0.001$), and both proxies show fluctuations that indicate frequent changes in clastic material inputs during the UKW event (Fig. 3, J and K).

4.3. Time-series analysis

Time-series analysis was conducted on the high-resolution (2–3 cm interval) XRF-derived Ti/Al record collected from the 4-m-thick interval from upper Frasnian to lower Famennian (Supplementary Fig. S5A). Multi-taper method (MTM) results in the stratigraphic domain reveal three major clusters of significant spectral peaks above the 95% confidence level: at ~0.7–0.9, ~12, ~14, ~22–23 cycles/m (Fig. 4A). Correlation coefficient (COCO) analysis yields two possible ranges of sedimentation rates (0.27–0.39 cm/kyr and 1.16–1.32 cm/kyr) with a correlation coefficient of >0.4 and a significance level of <0.01 to reject the null hypothesis (H_0, no astronomical forcing) (Supplementary Fig. S6, A and B). Sedimentation rates of 0.27–0.39 cm/kyr conform better to those estimates based on biostratigraphic data (i.e., ~0.2 cm/kyr; see details in Methods), and this range yields all seven astronomical components (Supplementary Fig. S6C; see details in Methods). The rate of 0.39 cm/kyr shows the highest correlation coefficient (Supplementary Fig. S6A) and is thus adopted as the optimal sedimentation rate. At this rate, the significant peaks at ~0.7–0.9, ~12, ~14 cycles/m are identified, which correspond to the ~405-kyr long-eccentricity cycle (Laskar et al., 2004), ~21-kyr obliquity cycle, and ~17-kyr precession cycle (Waltham, 2015), respectively (Fig. 4A). The significant peaks at ~22–23 cycles/m correspond to a cycle of ~12 kyr and probably represent half-precession cycles. In addition, no outstanding spectral peak (0.03 cycle/kyr) that represents the obliquity cycle (~34 kyr) is observed (Fig. 4A). We then applied the eFFT analysis to the Ti/Al stratigraphic-series profile. The eFFT results show a strong alignment with the eccentricity cycle and higher power in the precession band (Fig. 4B).

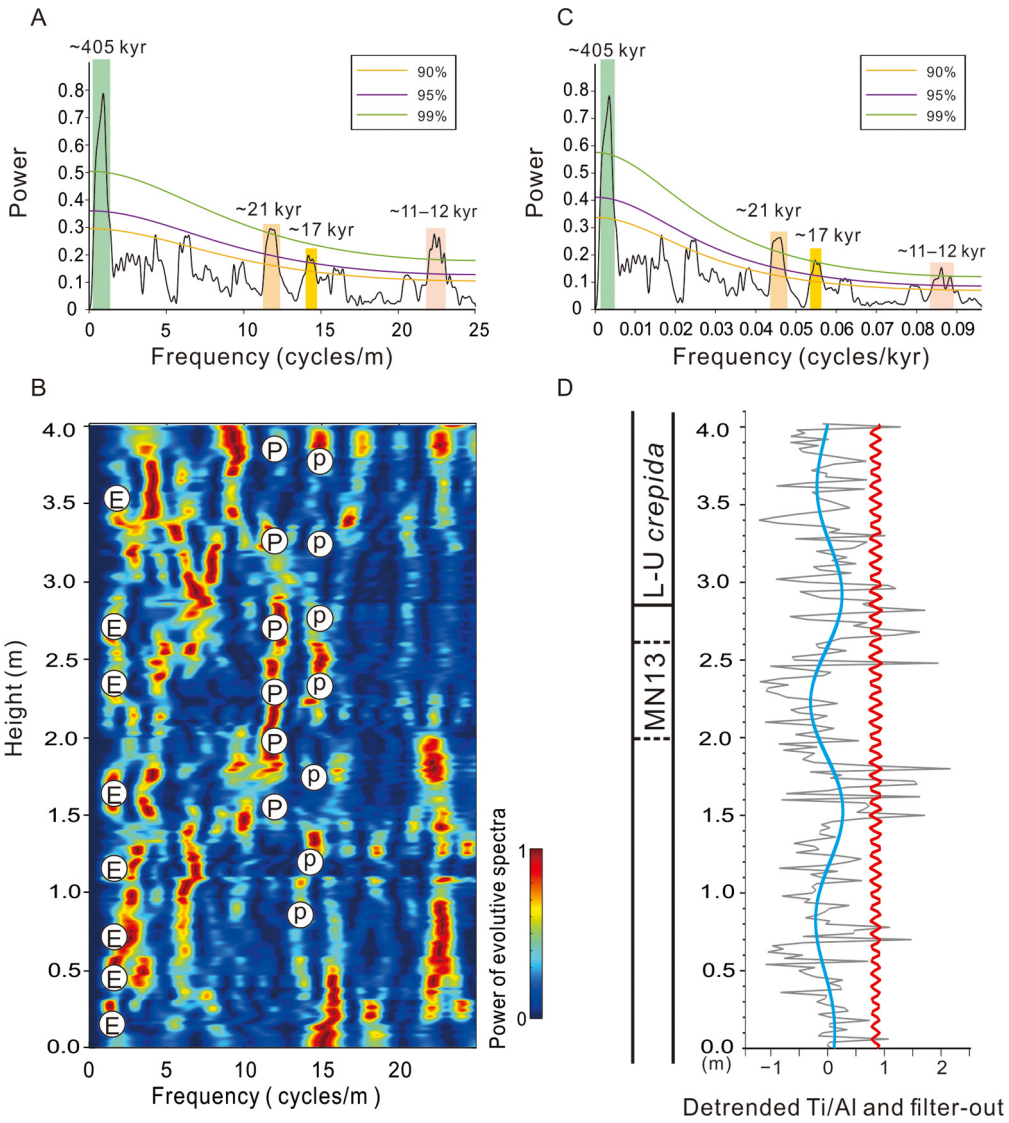

Fig. 4. Time-series analysis of a high-resolution XRF-derived Ti/Al record from a 4-m Upper Frasnian to Lower Famennian interval of the Chestnut Mound outcrop of the Chattanooga Shale, central Tennessee. (**A**) Results of 2π multiple-taper method (MTM) analysis in the stratigraphic domain. Numbers represent significant peaks shown in cycles/m; these peaks exceed the 95% confidence level (CL) based on the AR(1) red-noise model. (**B**) Evolutionary Fast Fourier transform (eFFT) spectrogram of the Ti/Al series. E: 405-kyr eccentricity, P: ~21-kyr precession, p: ~17-kyr precession. (**C**) Results of 2π MTM analysis of 405-kyr tuned Ti/Al series. Numbers represent significant peaks shown in cycles/kyr; these peaks exceed the 95% CL based on the AR(1) red-noise model. (**D**) Linear detrended Ti/Al data series (gray) filtered with the 405-kyr eccentricity cycle (blue) and the 21-kyr obliquity cycle (red). (For interpretation of the references to color in this figure legend, the reader is referred to the web version of this article.)

In order to construct an astronomical timescale, the data were converted from the stratigraphic domain to the time domain (Supplementary Fig. S5, B and C). Since the 405-kyr long-eccentricity cycle is the strongest periodicity observed (Fig. 4A), it was used to tune the Ti/Al record with 0.7 cycles/m assigned to 405-kyr periodicity. The MTM analysis of the tuned Ti/Al record sharpens the spectral peaks associated with the precession cycles (~21 and ~17 kyr), providing further evidence for the robustness of the identified precession cycles (Fig. 4C).

The bandpass filter generated visible astronomical cyclicities in the stratigraphic domain (Fig. 4D). Ti/Al ratios and other geochemical proxies for marine redox conditions, marine primary productivity, terrestrial plant and soil inputs all show fluctuations at spacings of ~8.5 cm and ~7 cm through the UKW interval (Fig. 3, L and M; Supplementary Fig. S3, D and E), suggesting rapid environmental oscillations that were significantly influenced by orbital cyclicity. The UKW interval of the Chestnut Mound section corresponds to five 17-kyr precession cycles, four 21-kyr precession cycles. Based on the tuning, we calculate a duration of ~1100 kyr for the 4-m-thick Ti/Al profile (Fig. 7A).

5. Discussion

5.1. Oceanic anoxia linked to terrestrial processes

Oceanic anoxic events indicated by the concentrations of intermediate-chain aryl isoprenoids (C_{18-20}) and the ratios of U/Th and V/(V+Ni) clearly display frequent fluctuations through the UKW interval (Fig. 3, C and D; Supplementary Fig. S3C), suggesting episodic development of PZE and oceanic anoxia/euxinia. This observation is in agreement with previous findings from other UKW sections around the world, including North America, Australia, Bolivia, China, Libya, and Poland (Fig. 1; Supplementary Table S1). Previous studies suggested that either excessive primary productivity (i.e., 'top-down' model) or the upwelling of anoxic deep waters (i.e., 'bottom-up' model) (e.g., Carmichael et al., 2019) could account for the occurrence of widespread oceanic anoxia during

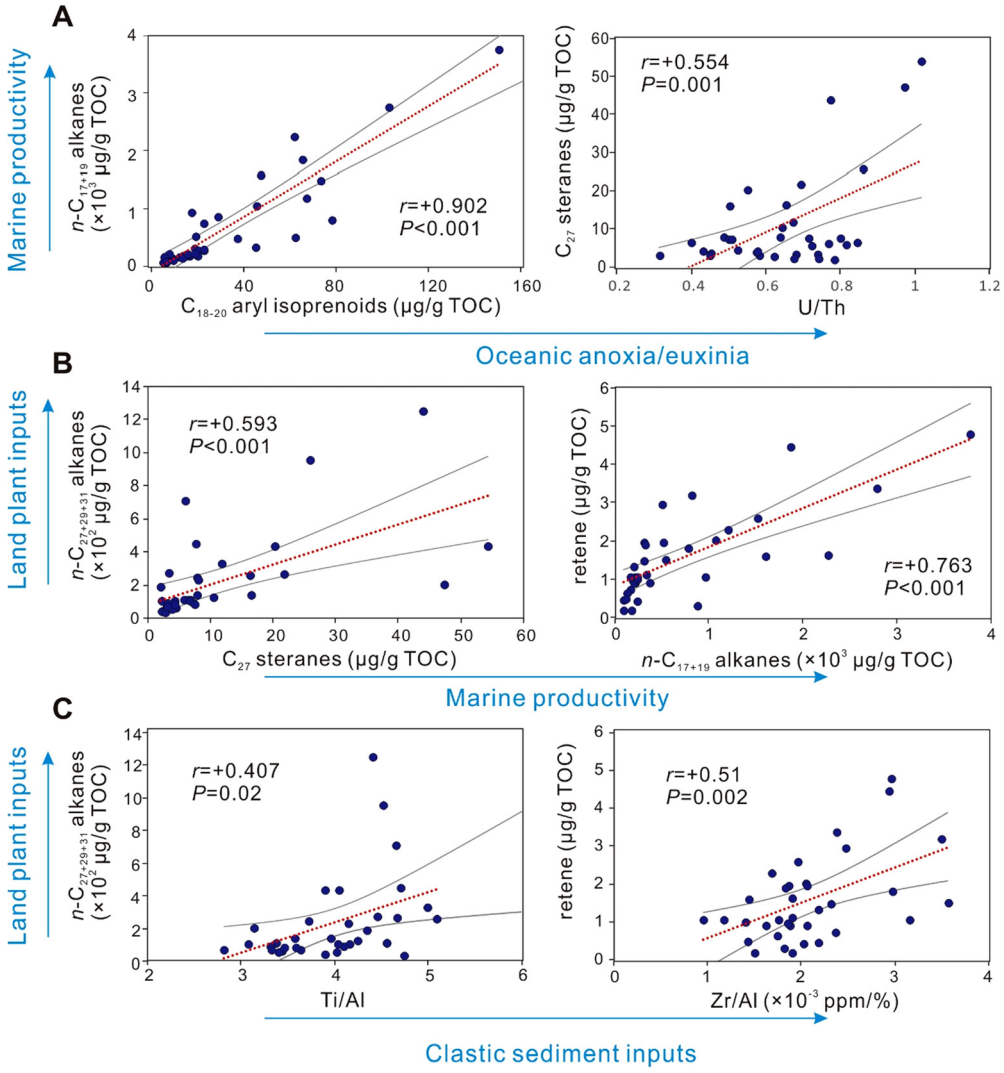

Fig. 5. Cross-plots of representative inorganic and organic geochemical proxies from the Upper Kellwasser (UKW) interval of the Chestnut Mound outcrop of the Chattanooga Shale, central Tennessee. (**A**) correlations between marine redox indices (C_{18-20} aryl isoprenoids, U/Th) and marine primary productivity indices (n-C_{17+19} alkanes, C_{27} steranes). (**B**) correlations between marine productivity indices and land plant biomarkers (n-$C_{27+29+31}$ alkanes, retene). (**C**) correlations between land plant biomarkers and clastic sediment input indices (Ti/Al, Zr/Al). Pearson's P and r values are shown. Red lines denote the best-fit linear regression line. Gray curve lines denote the 95% confidence interval.

the Late Devonian. The primary productivity-derived molecular biomarkers (n-C_{17+19} and C_{27} steranes) presented here support the 'top-down' model in the Appalachian Basin — both proxies show frequent fluctuations through the upper Frasnian (Fig. 3, E and F) and they covary significantly with indices for oceanic anoxia (Fig. 5A; Supplementary Table S3A). These observations suggest that intermittently elevated marine productivity, probably due to eutrophication, was the main factor triggering episodic anoxic/euxinic events during the UKW interval.

Episodic eutrophication during the UKW event could be further linked to pulsed inputs of land materials, as revealed by detailed inorganic and organic geochemical analyses. Land plant and soil-derived biomarkers also exhibit frequent fluctuations (Fig. 3, G to I; Supplementary Fig. S3, A and B) that covary positively with those of marine productivity indices (Fig. 5B; Supplementary Table S3B), suggesting the importance of terrestrial nutrients in eutrophication development. Furthermore, elevated fluxes of terrestrial organic matter coincided with the inputs of coarser clastic sediments, as shown by synchronous variations between terrestrial plant biomarkers and the ratios of Ti/Al and Zr/Al (Fig. 5C; Supplementary Table S3C). The grain size of clastic sediments varies with the strength of sediment mobilization and transport, and large grains often indicate greater weathering intensity and/or increasing riverine fluxes (Lash, 2017). Collectively, the pattern of synchronous, high-frequency co-variations of oceanic anoxia/euxinia and primary productivity with terrestrial organic and inorganic inputs strongly support the idea that land processes and associate terrestrial fluxes played a key role in the development of marine eutrophication and PZE. That is, the frequency and intensity of anoxic episodes were modulated by the strength of terrestrial-marine biogeochemical linkage. To test whether this model is applicable at a broad geographic scale for explaining the widespread continental shelf sea anoxia, high-resolution multi-proxy data beyond the Appalachian Basin are needed.

5.2. Astronomical-forcing mediated cycles in terrestrial-marine linkage

The time-series results presented here show prominent influence of precession during the UKW interval (Fig. 4; Supplementary Fig. S3). Precession cycles can modulate the input of terrestrial materials by mediating monsoonal precipitation and freshwater fluxes. During the Late Devonian, the paleolatitude of the study section is estimated to be 33°S (Fig. 1), a location where precessional influence dominates the fluctuations of incoming solar

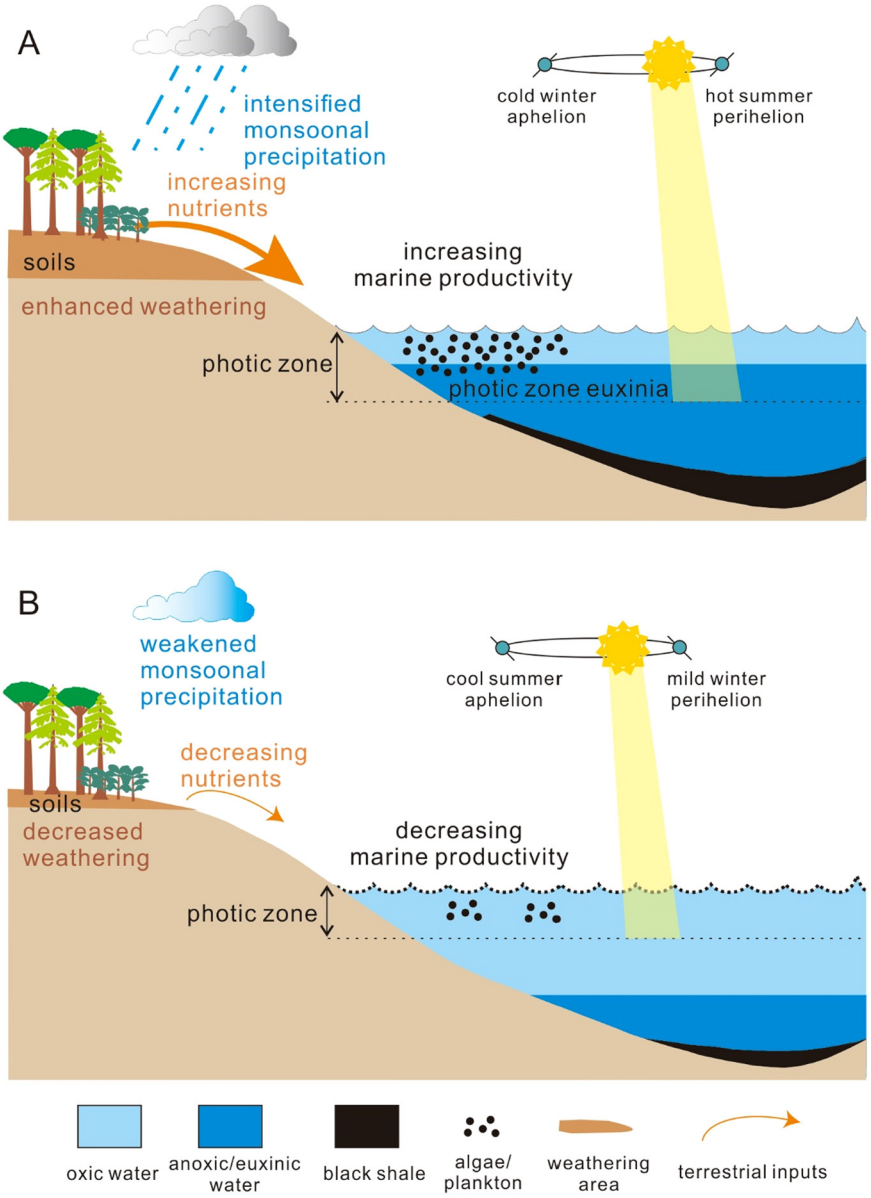

Fig. 6. Conceptual models of precession regulating the occurrence of oceanic anoxia via modulating land-ocean connectivity during the Late Devonian Upper Kellwasser (UKW) event. The seasonal references in the orbital configurations are for the Late Devonian Southern Hemisphere. (**A**) Intensified monsoons during the precession maximum enhanced terrestrial fluxes that lead to photic zone euxinia. (**B**) Weakened monsoons during the precession minimum reduced terrestrial fluxes and lead to an oxygenated ocean. (For interpretation of the references to color in this figure legend, the reader is referred to the web version of this article.)

radiation. Periods of precession maximum in the Southern Hemisphere correspond to hotter summers at perihelion and a stronger seasonal contrast (De Vleeschouwer et al., 2012). Consequently, summer monsoonal rainfalls were intensified, enhancing weathering intensity and river discharge and magnifying terrestrial inputs that led to higher marine productivity and oceanic anoxia/euxinia (Fig. 6A). In contrast, the precession minima reduced the seasonal contrast, thereby limiting rainfalls and the associated discharged of terrestrial materials to the ocean (Fig. 6B). Previously, De Vleeschouwer et al. (2017), based on time-series analysis of $\delta^{13}C$ of organic matter and carbonate, reported orbitally-controlled periodicity of the Late Devonian extinction intervals and noted a similar astronomical configuration for the Cretaceous Oceanic Anoxic Event-2, and they hence suggested a close link between astronomical forcing and global organic carbon burial could exist in general. Although $\delta^{13}C$ is a good tracer for global carbon cycle changes, it offers limited information on biogeochemical processes and mechanisms underlying organic carbon burial. The findings of the present study, derived from multiple provenance-specific or process-specific proxies, are significant in revealing the role of astronomical forcing in pacing the Late Devonian oceanic anoxic events through modulating the strength of land-ocean interactions.

Our data further show the influence of eccentricity from the Late Frasnian to Early Famennian (Fig. 4). This observation allows chemo-stratigraphically correlating the Chestnut Mound section with previously reported F–F sections across the globe. Previous studies, using Ti or magenetic susceptibility (MS) time-series profiles (both proxies can indicate detrital inputs, suggested that the UKW and LKW (Lower Kellwesser) are separated by one long-eccentricity cycle (~405 kyr) (Fig. 7) (De Vleeschouwer et al., 2017; Da Silva et al., 2020). The UKW interval of Chestnut Mound and other F–F sections all show highly variable Ti or MS values, with an increase and a high variability immediately following low values at the beginning of the UKW (Fig. 7). All LKW intervals are characterized by steeply increasing and highly variable Ti or MS values (Fig. 7).

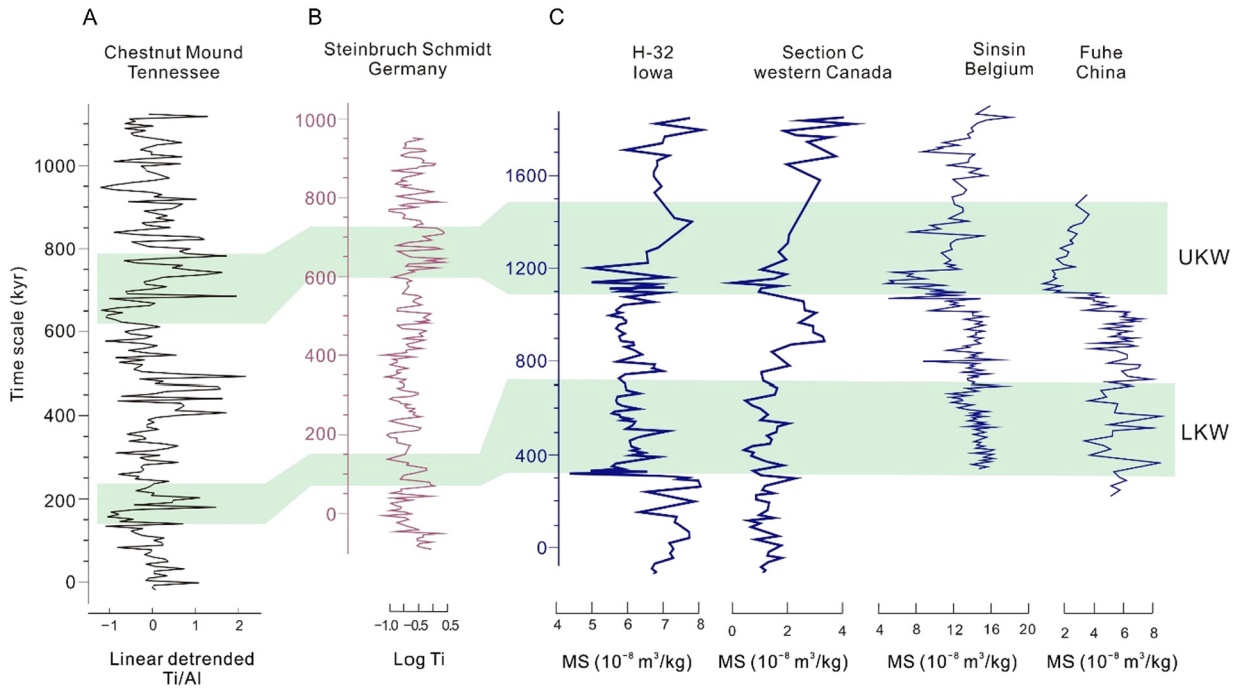

Fig. 7. Chemostratigraphic correlation of Chestnut Mound with five globally distributed Frasnian–Famennian (F–F) sections. (A) 405-kyr tuned Ti/Al series of the Chestnut Mound outcrop of the Chattanooga Shale, central Tennessee. (B) Log Ti profile of Steinbruch Schimidt section, Germany (adapted from Da Silva et al. (2020)). (C) Magnetic susceptibility profiles of four F–F sections (adapted from De Vleeschouwer et al. (2017)). Green bars highlight UKW (Upper Kellwasser) and LKW (Lower Kellwasser) intervals.

Two contrasting hypotheses have been proposed to explain the possible link between eccentricity and carbon cycle perturbations. The first argues that the eccentricity maxima can amplify the influence of precession (Rohling et al., 2015), which leads to a strong seasonal contrast that intensifies weathering and fluvial discharge and hence promotes organic carbon burial. This hypothesis is well integrated with the precessional influences observed in the Chestnut Mound UKW interval. The second hypothesis suggests that the eccentricity minimum favors organic carbon burial by lowering the seasonal contrast, which provides a stable condition for organic matter accumulation and preservation, including constant nutrient supplies, a steady level of marine productivity, and stratified water masses (Lanci et al., 2010).

5.3. Implications for the Late Devonian mass extinction

Despite some variation in the inferred intensity and secular pattern (most likely due to varying sampling resolutions), UKW anoxia has been identified as episodically occurring events pervading continental shelf seas around the world (Fig. 1; Supplementary Table S1). The periodicity of these events and the underlying mechanism, however, have not been firmly established in earlier studies. As such, how this periodic nature of anoxia/euxinia influenced the contemporaneous extinction patterns among marine organisms remains untested. Current data on the extinction timing and pattern do not yet have the scale of resolution that is necessary to answer this question. To date, no episodic extinction patterns at the strata- or layer-level within the UKW interval have been reported for any taxonomic groups. However, a five-stage extinction pattern was reported for the uppermost Frasnian or the UKW interval (McGhee, 2013). Some marine animal taxa also displayed a stepwise extinction process throughout the UKW interval in a specific site or region (e.g., Denayer and Edouard, 2010; Over et al., 2019). These studies documented a series of UKW extinctions, which argues against a single catastrophic cause (e.g., the Viluy Trap, the Alamo Impact, Ilyinets Impact, or Kaluga Impact) but favors a model based on recurrent environmental stressors, such as intermittent anoxia/euxinia synchronized globally by astronomical forcing. However, to further test and establish the anoxia-extinction linkage during the Late Devonian, future work must significantly improve the temporal resolution of both marine redox and extinction datasets by collecting samples at the highest-possible resolution through extinction intervals, as demonstrated in the present study.

Although astronomical forcing exists through the geological time, the tight linkage between such forcing and severe anoxia established here is a feature specific to the Late Devonian that provides new clues regarding the ultimate causal mechanism for UKW anoxia and extinction. For example, progressive volcanism is hypothesized to have been responsible for the intermittent pattern of oceanic anoxia during the Late Devonian (Racki et al., 2018), yet the frequency of volcanic activity is unlikely to have been connected to orbital cycles. Rather, volcanic eruptions may have altered the chemistry of terrestrial environments (e.g., fertilizing soils) that could contribute to eutrophication and anoxia through orbitally-paced land inputs. Similarly, processes that respond to astronomical forcing and operate through land-ocean interactions (e.g., river fluxes) are plausible candidates, including early land plant evolution, sea level fluctuation, and global cooling. The existing Late Devonian sea-level and temperature records (e.g., Joachimski and Buggisch, 2002) do not offer a sufficient temporal resolution to evaluate synchronicity (or desynchronicity) with oceanic anoxic episodes. On the other hand, the present study documented synchronous changes in oceanic redox conditions and terrestrial plant/soil fluxes, providing evidence for a significant global influence of early land plants (Fig. 6). The dominant arborescent lignophyte taxon of the Late Devonian (*Archaeopteris*) began to expand during the early Frasnian, and early forests were widely distributed across the eastern Euramerica by the late Frasnian (Lu et al., 2019). The initial radiation of forests is likely to have significantly altered terrestrial weathering patterns and liberated massive amounts of nutrients that were washed from continents into the ocean (Algeo and Scheckler, 1998). The present study area, i.e., southernmost Euramerica, was likely invaded by the early forests prior to the very

early Famennian (Lu et al., 2019). An expansion of the early forests, coupled with augmented terrestrial-to-marine fluxes paced by astronomical forcing, is likely to have been the trigger of recurrently lethal environmental conditions that were responsible for the UKW biotic crisis.

CRediT authorship contribution statement

Man Lu, YueHan Lu, and Yongge Sun designed this project. Data collection was performed by Man Lu, YueHan Lu, Takehitio Ikejiri, Dayang Sun, Richard Carroll, Elliot H. Blair and Yongge Sun. Man Lu, YueHan Lu, and Yongge Sun wrote the early draft of the manuscript, and all authors contributed to the improvement and revision of the manuscript.

Declaration of competing interest

The authors declare that they have no known competing financial interests or personal relationships that could have appeared to influence the work reported in this paper.

Data and materials availability

All data needed to evaluate the conclusions in the paper are present in the paper and/or the Supplementary Materials. Additional data related to this paper may be requested from the authors.

Acknowledgements

Acknowledgments are made to the Donors of American Chemical Society Petroleum Research Fund (PRF#61366-ND2 to YueHan Lu). We also acknowledge the support from the Gulf Coast Association of Geological Societies (to YueHan Lu and Man Lu). YueHan Lu thanks the six-month Sabbatical Fellowship from the South University of Science and Technology of Shen Zhen, China. We thank Xinguang Wang, Huijing Fang and Xiaoting Liu for field assistance. We thank Dr. Louis Derry, Dr. David DeVleeschouwer and one anonymous reviewer for detailed and thoughtful reviews. We would like to thank Dr. Mingsong Li for assisting with data processing. The biomarker analyses were performed on a GC-MS purchased through the support from the Instrumentation and Facilities Programs in the Division of Earth Sciences to Y.H.L. (NSF EAR-1255724) YL and TI acknowledge Dr. Paul Aharon for numerous stimulating discussions on the Devonian.

Appendix A. Supplementary material

Supplementary material related to this article can be found online at https://doi.org/10.1016/j.epsl.2021.116839.

References

Algeo, T.J., Scheckler, S.E., 1998. Terrestrial-marine teleconnections in the Devonian: links between the evolution of land plants, weathering processes, and marine anoxic events. Philos. Trans. R. Soc. Lond. B, Biol. Sci. 353, 113–130. https://doi.org/10.1098/rstb.1998.0195.

Averbuch, O., Tribovillard, N., Devleeschouwer, X., Riquier, L., Mistiaen, B., Van Vliet-Lanoe, B., 2005. Mountain building-enhanced continental weathering and organic carbon burial as major causes for climatic cooling at the Frasnian–Famennian boundary (c. 376 Ma)? Terra Nova 17, 25–34. https://doi.org/10.1111/j.1365-3121.2004.00580.x.

Bambach, R.K., Knoll, A.H., Wang, S.C., 2004. Origination, extinction, and mass depletions of marine diversity. Paleobiology 30, 522–542. https://doi.org/10.1666/0094-8373(2004)030<0522:OEAMDO>2.0.CO;2.

Boyer, D.L., Haddad, E.E., Seeger, E.S., 2014. The last gasp: trace fossils track deoxygenation leading into the Frasnian–Famennian Extinction Event. Palaios 29, 646–651. https://doi.org/10.2110/palo.2014.049.

Bush, R.T., McInerney, F.A., 2013. Leaf wax *n*-alkane distributions in and across modern plants: implications for paleoecology and chemotaxonomy. Geochim. Cosmochim. Acta 117, 161–179. https://doi.org/10.1016/j.gca.2013.04.016.

Carmichael, S.K., Waters, J.A., Königsof, P., Suttner, T.J., Kido, E., 2019. Paleogeography and paleoenvironments of the Late Devonian Kellwasser event: a review of its sedimentological and geochemical expression. Glob. Planet. Change 183, 102984. https://doi.org/10.1016/j.gloplacha.2019.102984.

Copper, P., 2002. Reef development at the Frasnian/Famennian mass extinction boundary. Palaeogeogr. Palaeoclimatol. Palaeoecol. 181, 27–65. https://doi.org/10.1016/S0031-0182(01)00472-2.

Da Silva, A.C., Sinnesael, M., Claeys, P., Davies, J.H., de Winter, N.J., Percival, L.M.E., Schaltegger, U., De Vleeschouwer, D., 2020. Anchoring the Late Devonian mass extinction in absolute time by integrating climatic controls and radio-isotopic dating. Sci. Rep. 10, 1–12. https://doi.org/10.1038/s41598-020-69097-6.

De Vleeschouwer, D., Da Silva, A.C., Boulvain, F., Crucifix, M., Claeys, P., 2012. Precessional and half-precessional climate forcing of Mid-Devonian monsoon-like dynamics. Clim. Past 8, 337–351. https://doi.org/10.5194/cp-8-337-2012.

De Vleeschouwer, D., Rakociński, M., Racki, G., Bond, D.P., Sobień, K., Claeys, P., 2013. The astronomical rhythm of late-Devonian climate change (Kowala section, Holy Cross Mountains, Poland). Earth Planet. Sci. Lett. 365, 25–37. https://doi.org/10.1016/j.epsl.2013.01.016.

De Vleeschouwer, D., Da Silva, A.C., Sinnesael, M., Chen, D., Day, J.E., Whalen, M.T., Guo, Z., Claeys, P., 2017. Timing and pacing of the Late Devonian mass extinction event regulated by eccentricity and obliquity. Nat. Commun. 8, 2268. https://doi.org/10.1038/s41467-017-02407-1.

Denayer, J., Edouard, P., 2010. Facies and palaeoecology of the upper member of the Aisemont Formation (Late Frasnian, S. Belgium): an unusual episode within the Late Frasnian crisis. Geol. Belg. 13, 197–212. https://popups.uliege.be:443/1374-8505/index.php?id=2935.

Eglinton, G., Hamilton, R.J., 1967. Leaf epicuticular waxes. Science 156, 1322–1335. https://doi.org/10.1126/science.156.3780.1322.

Elrick, M., Berkyová, S., Klapper, G., Sharp, Z., Joachimski, M., Frýda, J., 2009. Stratigraphic and oxygen isotope evidence for My-scale glaciation driving eustasy in the Early–Middle Devonian greenhouse world. Palaeogeogr. Palaeoclimatol. Palaeoecol. 276, 170–181. https://doi.org/10.1016/j.palaeo.2009.03.008.

Fenton, S., Grice, K., Twitchett, R.J., Böttcher, M.E., Looy, C.V., Nabbefeld, B., 2007. Changes in biomarker abundances and sulfur isotopes of pyrite across the Permian–Triassic (P/Tr) Schuchert Dal section (East Greenland). Earth Planet. Sci. Lett 262, 230–239. https://doi.org/10.1016/j.epsl.2007.07.033.

Golonka, J., 2020. Late Devonian paleogeography in the framework of global plate tectonics. Glob. Planet. Change 186, 103129. https://doi.org/10.1016/j.gloplacha.2020.103129.

Grice, K., Cao, C., Love, G.D., Böttcher, M.E., Twitchett, R.J., Grosjean, E., Summons, R.E., Turgeon, S.C., Dunning, W., Jin, Y., 2005. Photic zone euxinia during the Permian-Triassic superanoxic event. Science 307, 706–709. https://doi.org/10.1126/science.1104323.

Haddad, E.E., Tuite, M.L., Martinez, A.M., Williford, K., Boyer, D.L., Droser, M.L., Love, G.D., 2016. Lipid biomarker stratigraphic records through the Late Devonian Frasnian/Famennian boundary: comparison of high- and low-latitude epicontinental marine settings. Org. Geochem. 98, 38–53. https://doi.org/10.1016/j.orggeochem.2016.05.007.

Han, J., Mccarthy, E., Calvin, M., Benn, M., 1968. Hydrocarbon constituents of the blue-green algae *Nostoc muscorum*, *Anacystis nidulans*, *Phormidium luridium* and *Chlorogloea fritschii*. J. Chem. Soc. C, Organic, 2785–2791. https://doi.org/10.1039/J39680002785.

House, M.R., 2002. Strength, timing, setting and cause of mid-Palaeozoic extinctions. Palaeogeogr. Palaeoclimatol. Palaeoecol. 181, 5–25. https://doi.org/10.1016/S0031-0182(01)00471-0.

Joachimski, M.M., Buggisch, W., 1993. Anoxic events in the late Frasnian—causes of the Frasnian-Famennian faunal crisis? Geology 21, 675–678. https://doi.org/10.1130/0091-7613(1993)021<0675:AEITLF>2.3.CO;2.

Joachimski, M.M., Buggisch, W., 2002. Conodont apatite δ^{18}O signatures indicate climatic cooling as a trigger of the Late Devonian mass extinction. Geology 30, 711–714. https://doi.org/10.1130/0091-7613(2002)030<0711:CAOSIC>2.0.CO;2.

Joachimski, M.M., Pancost, R., Freeman, K.H., Ostertag-Henning, C., Buggisch, W., 2002. Carbon isotope geochemistry of the Frasnian–Famennian transition. Palaeogeogr. Palaeoclimatol. Palaeoecol. 181, 91–109. https://doi.org/10.1016/S0031-0182(01)00474-6.

Kaufmann, B., 2006. Calibrating the Devonian Time Scale: a synthesis of U–Pb ID–TIMS ages and conodont stratigraphy. Earth-Sci. Rev. 76, 175–190. https://doi.org/10.1016/j.earscirev.2006.01.001.

Kodama, K.P., Hinnov, L.A., 2014. Rock Magnetic Cyclostratigraphy. John Wiley & Sons.

Kodner, R.B., Pearson, A., Summons, R.E., Knoll, A.H., 2008. Sterols in red and green algae: quantification, phylogeny, and relevance for the interpretation of geologic steranes. Geobiology 6, 411–420. https://doi.org/10.1111/j.1472-4669.2008.00167.x.

Lanci, L., Muttoni, G., Erba, E., 2010. Astronomical tuning of the Cenomanian Scaglia Bianca Formation at Furlo, Italy. Earth Planet. Sci. Lett. 292, 231–237. https://doi.org/10.1016/j.epsl.2010.01.041.

Lash, G.G., 2017. A multiproxy analysis of the Frasnian–Famennian transition in western New York State, USA. Palaeogeogr. Palaeoclimatol. Palaeoecol. 473, 108–122. https://doi.org/10.1016/j.palaeo.2017.02.032.

Laskar, J., Robutel, P., Joutel, F., Gastineau, M., Correia, A., Levrard, B., 2004. A long-term numerical solution for the insolation quantities of the Earth. Astron. Astrophys. 428, 261–285. https://doi.org/10.1051/0004-6361:20041335.

Li, M., Hinnov, L., Kump, L., 2019. Acycle: time-series analysis software for paleoclimate research and education. Comput. Geosci. 127, 12–22. https://doi.org/10.1016/j.cageo.2019.02.011.

Li, Y., Schieber, J., 2015. On the origin of a phosphate enriched interval in the Chattanooga Shale (Upper Devonian) of Tennessee—a combined sedimentologic, petrographic, and geochemical study. Sediment. Geol. 329, 40–61. https://doi.org/10.1016/j.sedgeo.2015.09.005.

Liu, J., Algeo, T.J., Jaminski, J., Kuhn, T., Joachimski, M.M., 2019. Evaluation of high-frequency paleoenvironmental variation using an optimized cyclostratigraphic framework: example for C-S-Fe analysis of Devonian-Mississippian black shales (Central Appalachian Basin, U.S.A.). Chem. Geol. 525, 303–320. https://doi.org/10.1016/j.chemgeo.2019.07.019.

Lu, M., Lu, Y., Ikejiri, T., Hogancamp, N., Sun, Y., Wu, Q., Carroll, R., Çemen, I., Pashin, J., 2019. Geochemical evidence of First Forestation in the southernmost euramerica from Upper Devonian (Famennian) Black shales. Sci. Rep. 9, 7581. https://doi.org/10.1038/s41598-019-43993-y.

Lu, Y., Hautevelle, Y., Michels, R., 2013. Determination of the molecular signature of fossil conifers by experimental palaeochemotaxonomy-Part 1: the Araucariaceae family. Biogeosciences 10, 1943–1962. https://doi.org/10.5194/bg-10-1943-2013.

Mann, M.E., Lees, J.M., 1996. Robust estimation of background noise and signal detection in climatic time series. Clim. Change 33, 409–445. https://doi.org/10.1007/BF00142586.

Marynowski, L., Simoneit, B.R., 2009. Widespread Upper Triassic to Lower Jurassic wildfire records from Poland: evidence from charcoal and pyrolytic polycyclic aromatic hydrocarbons. Palaios 24, 785–798. https://doi.org/10.2110/palo.2009.p09-044r.

McGhee, G.R., 2013. When the Invasion of Land Failed: The Legacy of the Devonian Extinctions. Columbia University Press.

Over, D.J., 2002. The Frasnian/Famennian boundary in central and eastern United States. Palaeogeogr. Palaeoclimatol. Palaeoecol. 181, 153–169. https://doi.org/10.1016/S0031-0182(01)00477-1.

Over, D.J., 2007. Conodont biostratigraphy of the Chattanooga Shale, Middle and Upper Devonian, southern Appalachian Basin, eastern United States. J. Paleontol. 81, 1194–1217. https://doi.org/10.1666/06-056R.1.

Over, D.J., Hauf, E., Wallace, J., Chiarello, J., Over, J.S., Gilleaudeau, G.J., Song, Y., Algeo, T.J., 2019. Conodont biostratigraphy and magnetic susceptibility of Upper Devonian Chattanooga Shale, eastern United States: evidence for episodic deposition and disconformities. Palaeogeogr. Palaeoclimatol. Palaeoecol. 524, 137–149. https://doi.org/10.1016/j.palaeo.2019.03.017.

Racki, G., Rakociński, M., Marynowski, L., Wignall, P.B., 2018. Mercury enrichments and the Frasnian-Famennian biotic crisis: a volcanic trigger proved? Geology 46, 543–546. https://doi.org/10.1130/G40233.1.

Riquier, L., Tribovillard, N., Averbuch, O., Joachimski, M.M., Racki, G., De Vleeschouwer, X., Riboulleau, A., 2005. Productivity and bottom water redox conditions at the Frasnian-Famennian boundary on both sides of the Eovariscan Belt: constraints from trace-element geochemistry. In: Over, D.J., Morrow, J.R., Wignall, P.B. (Eds.), Developments in Palaeontology and Stratigraphy. Elsevier, pp. 199–224.

Rohling, E.J., Marino, G., Grant, K.M., 2015. Mediterranean climate and oceanography, and the periodic development of anoxic events (sapropels). Earth-Sci. Rev. 143, 62–97. https://doi.org/10.1016/j.earscirev.2015.01.008.

Sageman, B.B., Murphy, A.E., Werne, J.P., Ver Straeten, C.A., Hollander, D.J., Lyons, T.W., 2003. A tale of shales: the relative roles of production, decomposition, and dilution in the accumulation of organic-rich strata, Middle–Upper Devonian, Appalachian basin. Chem. Geol. 195, 229–273. https://doi.org/10.1016/S0009-2541(02)00397-2.

Sandberg, C.A., Morrow, J.R., Ziegler, W., 2002. Late Devonian Sea-Level Changes, Catastrophic Events, and Mass Extinctions. Geol. Soc. Am. Spec. Pap., vol. 356, pp. 473–488.

Schwark, L., Empt, P., 2006. Sterane biomarkers as indicators of Palaeozoic algal evolution and extinction events. Palaeogeogr. Palaeoclimatol. Palaeoecol. 240, 225–236. https://doi.org/10.1016/j.palaeo.2006.03.050.

Sephton, M.A., Looy, C.V., Brinkhuis, H., Wignall, P.B., De Leeuw, J.W., Visscher, H., 2005. Catastrophic soil erosion during the end-Permian biotic crisis. Geology 33, 941–944. https://doi.org/10.1130/G21784.1.

Thomson, D.J., 1982. Spectrum estimation and harmonic analysis. Proc. IEEE 70, 1055–1096. https://doi.org/10.1109/PROC.1982.12433.

Waltham, D., 2015. Milankovitch period uncertainties and their impact on cyclostratigraphy. J. Sediment. Res. 85, 990–998. https://doi.org/10.2110/jsr.2015.66.

Whalen, M.T., De Vleeschouwer, D., Payne, J.H., Day, J., Over, D.J., Claeys, P., 2017. Pattern and timing of the Late Devonian biotic crisis in Western Canada: insights from carbon isotopes and astronomical calibration of magnetic susceptibility data. In: Playton, E., Kerans, C., Weissenberger, J.A.W. (Eds.), New Advances in Devonian Carbonates: Outcrop Analogs, Reservoirs, and Chronostratigraphy. Society for Sedimentary Geology, pp. 185–201.